Functional Network Connectivity Analysis in Absence Epilepsy Using Stargazer Mice

Andreas Zacharakis*†, Manthos Kampourakis†, Orestis Mousouros*†, Ganna Palagina‡¶
Jochen Meyer§, Ioannis Smyrnakis†, Stelios Manolis Smirnakis‡¶ and Maria Papadopouli*†‖
*Department of Computer Science, University of Crete, Heraklion, Greece
†Institute of Computer Science, Foundation for Research and Technology-Hellas, Heraklion, Greece
‡Brigham and Womens Hospital, Harvard Medical School, Boston, MA 02115
§Department of Neurology, Baylor College of Medicine, One Baylor Plaza, Houston, TX, USA
¶Boston VA Research Institute, Jamaica Plain Veterans Administration Hospital, Harvard Medical School, Boston, United States

***Abstract*—Absence epilepsy is a common childhood disorder featuring frequent cortical spike-wave seizures with a loss of awareness and behavior. Using the calcium indicator GCaMP6 with in vivo 2-photon cellular microscopy and simultaneous electrocorticography, we examined the collective activity profiles of individual neurons and surrounding neuropil patches in layer 2/3 (L2/3) of the visual cortex during spike-wave seizure activity over prolonged periods in 2 different stargazer mice. Our long-term objective is to predict in real-time a seizure. In this work, we focused on identifying the neuronal networks activated during epochs of interictal activity (i.e., between seizure activities) and seizure activity and analyzed their functional network connectivity. During interictal activity, most neurons are functionally connected with a large number of neighbors within the field of view, while in seizure epochs, the connectivity is reduced substantially. We also examined the discriminating power of groups of neurons in identifying seizure events. An SVM model based on the firing activity of neurons can reasonably accurately classify the interictal activity vs. seizure (e.g., 77.9% for the total accuracy with sensitivity equal to 85.3%, and specificity 73%).**

I. Introduction

Absence epilepsy [1], [2] interrupts normal cortical processing, producing reversible episodes of altered consciousness. Each seizure begins without warning, replacing planned motor movements with speech arrest and a vacant stare lasting only a few seconds, followed by sudden and complete recovery of awareness and intentional behavior. These events can provide unique functional insight into the coupling of human perception and volition. The stargazer model, one of over 20 monogenic mouse mutants with this phenotype [1], displays frequent, recurrent spike-wave seizures with behavioral arrest. Prior work in humans and animal models of absence epilepsy present at times conflicting evidence of where and how cortical activity is modulated during absence seizures.

This work has been funded from the Hellenic Foundation for Research and Innovation (HFRI) and the General Secretariat for Research and Technology (GSRT) under grant agreement No 2285, the Fondation Sante FORTH-ICS E00120, the Erasmus+ International Mobility between University of Crete and Harvard Medical School 2017-1-EL01-KA107-035639, the Marie Curie RISE NHQWAVE project under grant agreement No 4500, and the NINDS R21 NS088457.

‖Contact author: Maria Papadopouli (mgp@ics.forth.gr)

Here, simultaneously recorded electrocorticography (ECoG) and 2-photon microscopy measurements are employed to study cortical patterns of neuronal activity that emerge in cortical layer 2/3 during absence seizures versus epochs of interictal activity.

The identification of patterns of neuronal synchrony (the so called functional connectivity [3]) reflects underlying direct or indirect interaction across pairs of neurons as well as distinct neuronal sub-networks. Neurons within each layer do not fire independently from each other but rather form computationally meaningful interconnected neuronal ensembles. Our long-term objective is to predict in real-time a seizure event. The focus of this work is to map and compare functional connectivity patterns in cortical layer 2/3 during epochs of interictal activity versus absence seizure activity, and then use this information to predict in real-time a seizure event. We therefore examine the discriminating power that the firing activity of layer 2/3 neuronal ensembles has in classifying interictal activity versus seizure events.

Two neurons are functionally connected, if their firing activity has a statistically significant temporal correlation. The correlation measure has to be chosen carefully, to take into consideration of the special features of spike trains. For relatively long time-series, Spike Time Tiling Coefficient (STTC) [4] is superior to commonly used measures, including Pearson, as it accounts for relative time shifts, local fluctuations of neural activity or noise, and the presence of periods without firing events. Here we use STTC to identify and characterize the functional networks that are present during seizures versus interictal activity, for different statistical thresholds. We found distinct interneuronal STTC profiles during epochs of seizure versus interictal. Morerover, the functional connectivity is reduced substantially among neurons and neuropil patches during seizure. Similar to Meyer *et al.* [5] (who used Pearson correlation), we found that functional connectivity among pairs of neurons and neuropil patches was reduced substantially during seizures. STTC analysis adds a more finely graded understanding of how cortical L2/3 functional correlations behave during the transitions from interictal periods to absence seizures.

We were able to accurately identify periods of seizure versus interictal activity. Specifically, an SVM classifier can accurately classify windows of interictal activity vs. seizure, achieving total mean accuracy of 77.9% (85.3% sensitivity, 73% specificity), in 15-fold cross validation.

Section III describes briefly the 2-photon measurements. In Section IV, we focus on the temporal correlation and network analysis, while Section V discusses the preliminary results on the discriminating power of groups of neurons for identifying seizure vs. interictal activity epochs using SVM. Section VI summarizes the main results and future work plans.

II. Related Work

The stargazer model, one of over 20 monogenic mouse mutants with this phenotype [1], displays frequent, recurrent spike-wave seizures with behavioral arrest that are sensitive to blockade by ethosuximide [6]. Loss of the transmembrane AMPA receptor regulatory protein (TARP) subunit Cacng2 in stargazer mice leads to mistrafficking of dendritic AMPA receptors in fast-spiking interneurons in the neocortex [7] and thalamus [8], [9] and to remodeling of firing properties in thalamocortical circuitry that favor abnormal oscillations [9]. This loss of inhibition, particularly feedforward inhibition, is implicated in the pathophysiology of most monogenic models of absence epilepsy [2], [10]. However, how cortical neurons are engaged in absence seizure events is not known in detail, and indeed existing evidence appears at times conflicting.

While several studies in rats showed no activity changes in visual cortex [11] or in somatosensory and motor cortex [12], functional magnetic resonance imaging (fMRI) studies in humans have demonstrated increased ictal blood oxygen level-dependent (BOLD) activity in the occipital cortex [13] or biphasic activation and deactivation of large scale networks, including visual cortex [14], [15].

Cortical network activity at single cell resolution is not well understood during absence seizure events. Recent results by Meyer al. [5] showed that the majority of neurons in all cortical layers reduces their activity during absence seizures. Inter-neuronal Pearson correlation of 2-photon data acquired in vivo revealed a surprising lack of synchrony among neurons and neuropil patches in all layers during seizure. Here we analyze layer 2/3 cortical functional connectivity patterns in more detail and study whether we can use them to identify and discriminate epochs of seizure versus interictal activity.

III. Collected datasets

Simultaneously recorded electrocorticography (EcoG) and 2-photon microscopy measurements are employed to study cortical patterns of neuronal activity that emerge in cortical layer 2/3 during absence seizures versus epochs of interictal activity. EcoG is just another reference to epidural EEG recording as described as follows: 1 mm long, flat Ag/Ag-Cl electrodes were placed epidurally over the ipsilateral somatosensory cortex, 2mm anterior to the middle of the craniotomy, and over the contralateral visual cortex; and a titanium headpost was permanently attached with dental cement. A reference electrode was implanted over the contralateral cerebellar hemisphere. During imaging sessions, the EEG signal was sampled at 2 or 5 kHz with filtering cut-offs set at 1 Hz and 250 Hz. Seizures were detected by visual inspection by an experienced user (AM) in MATLAB (EEGLab) according to specific criteria (regular spike-wave burst structure, spike amplitude 1.5 baseline, spike frequency of 59 Hz, and a minimum duration of 0.5 s). The peaks of the first and last EEG spike were considered as the seizure onset and offset, respectively.

Calcium data were collected from layer 2/3 of area V1, as described in Meyer *et al.* [5]. Two animals were analyzed here (i.e., mice A, B). Raw calcium traces for regions of interest (ROIs), namely, neuronal cell bodies and neuropil patches, were created using the mean of all pixel intensities inside an ROI, and then high-pass filtered (0.1 Hz) and normalized by their individual baselines to ΔF/F values. To differentiate calcium transients from baseline fluctuations, the baseline (F) at time point t was defined as the mean of the bottom 10% of all data points within t$\pm$20 s.

Firing rates were extrapolated from the ΔF/F traces using a modified version of 2 different deconvolution methods [16], [17], yielding consistent results. The method used to deconvolve the data we present here was based on a previously published method [16] that uses (1) an iterative smoothing process to remove local low amplitude peaks representing noise without distorting the ΔF/F signal stemming from calcium fluctuations, and (2) inverse filtering of the smoothed traces with an exponential kernel.

The fluorescence signal f recorded through two photon microscopy from neurons is deconvolved to obtain an estimated spike using the deconvolution algorithm, which reports the most probable spike train given the Calcium signal recorded. A linear dependence of the fluorescence on the Calcium concentration is assumed. This calcium concentration is taken to decay exponentially to the calcium baseline upon excitation. A well-known issue of this method is that it does not produce a binary spike train (i.e. eventogram), but it rather gives an analog output s that represents the probability of spike existence at all frames. To turn this into an eventogram a threshold is used. If the analog output is above the threshold a spike (event) is inserted, otherwise the analog output is ignored. The threshold is set through the assignment of noise intervals on the raw fluorescence signal. This is done under the assumption of low firing rates ($<$ 1Hz). Under this assumption, the median fluorescence value f_{med} corresponds to no spike, hence to noise. To find secure noise intervals in the fluorescence recording, we take only the bins where the fluorescence value is below the median, $f(i) < f_{med}$. The collection of these bins forms the union of noise intervals I_{noise}. Once the noise intervals I_{noise} are obtained, we restrict the deconvolution output signal s on these intervals. This restricted signal is noise signal, but it is also constrained to have values below the median f_{med}.

To get a more representative noise signal, we create another artificial copy of I_{noise} over which we assign reflected fluores-

cence values w.r.t f_{med}, producing the noise signal s_{noise}. This reconstructed signal corresponds to noise, since it is projected from noise intervals in the Calcium signal. The threshold used for the analog output signal of the deconvolution is based on the standard deviation of s_{noise}. For a recording of the order of 3000 bins a reasonable threshold is 3 standard deviations above the mean of s_{noise}. If we assume that s_{noise} is normally distributed around the mean, then this threshold will only allow approx. 10 incorrect spikes arising from noise. The thresholded output s_{bin} is the output of the deconvolution procedure that we used.

Meyer *et al*. [5] empirically determined a minimum level of activity for an ROI below which it was not possible to determine whether the ROI had statistically significant firing events due to lack of data points, by calculating the sum of noise-corrected ΔF/F signal per minute for each ROI. ROIs with mean activity below this threshold were deemed quiet and excluded from further analysis. The remaining ROIs were then used for the analysis and are the neurons we report on here. Specifically, ROIs of 1 to 54 are the neurons, while 55-64 are the neuropil patches. For each ROI, there is a corresponding time-series of frames that provides a reasonable approximation of spiking. Note that it does not indicate the single spikes but rather whether there was calcium activity or not for each imaging frame: Each frame of activity could be result of one or several spikes at a time. More information about the experiments and the data collection process can be found in [5].

IV. STTC Analysis

STTC quantifies the temporal correlation between spike trains [4]. Specifically, for the estimation of the STTC between spike trains A and B, it computes the proportion of total recording time which lies within $\pm\Delta$t of any spike of the spike trains of A and B, T_A and T_B, respectively. Then, it computes the proprtion of spikes from A, which lie within $\pm\Delta$t of any spike from B (P_A). P_B is calculated similarly. The spike time tiling coefficient can be defined by:

$$STTC = \frac{1}{2}\Big(\frac{P_a - T_b}{1 - P_a T_b} + \frac{P_b - T_a}{1 - P_b T_a}\Big) \tag{1}$$

The STTC is positive if spikes in train A are correlated with spikes from train B, and negative if there is less correlation than expected by chance. The normalization factor (1 - $P_a T_b$) ensures that STTC is in the range of [-1, 1].

For each pair of neurons (i,j), we estimate its (observed) STTC value ($STTC_{i,j}^{obs}$) as well as the control which corresponds to the chance level (null). We consider *synchronous* firing between neurons (i.e., two neurons exhibit a firing event within the same frame). For the estimation of the control, for each pair (i, j), we circularly reshuffle j by a randomly selected number (in the range of $[1, T]$, where T is the length of the spike train). This corresponds to a new spike train j'. We estimate the STTC between i and j'. We repeat this process 500 times. This corresponds to the control (null) distribution. The mean $\overline{STTC_{i,j}^{null}}$ and standard deviation $\sigma_{i,j}^{null}$ of the control, for each pair (i, j) are estimated. The neurons (i, j) have a statistical significant temporal correlation (i.e., are connected with an edge), if their STTC value $STTC_{i,j}^{obs}$ is above a certain z-value threshold, a:

$$\frac{STTC_{i,j}^{obs} - \overline{STTC_{i,j}^{null}}}{\sigma_{i,j}^{null}} > a \tag{2}$$

For each neuron, we constructed a time series during interictal activity (seizure) by concatenating all frames in interictal activity (seizure), respectively. We then estimated the STTC values for all pairs of neurons in interictal activity as well as in seizure considering their corresponding time series. Thus, for each pair of neurons, we estimated two observed STTC values: the observed STTC value during the interictal activity and the one during seizure (Fig.1).

Distinct pairwise correlation profiles during epochs of interictal activity versus absence seizure activity. STTC value profiles (cdfs) are significantly different than the null distributions in both normal and seizure epochs (as shown in Fig. 1, for different z-score thresholds). Fig. 1 illustrates the prominent deviation that observed STTC profiles have from the corresponding null distributions (the dotted lines represent 500 circularly shuffled repetitions overlaid on each other). The mean of the null distribution of STTC values in the interictal epoch is 0 and the standard deviation of this distribution is very tight at 0.01. During seizure epochs, the STTC values of most pairs of neurons is relatively low. For example, for threshold 4, during seizure epochs, 90% of pairs of neurons with a statistical significant connection, have STTC value equal or below 0.07 (Fig. 1). Furthermore, the STTC profile obtained during interictal epochs (green) differs from the one obtained during absence seizures (red) (see also Fig. 8, left column). Specifically, during absence seizure epochs, most STTC values remain relatively low.

During interictal activity, there is high neuronal degree of connectivity. The *degree of connectivity* of a neuron is the number of statistical significant functional connections that it has with other neurons. For small thresholds, the majority of neurons have high degree of connectivity (Fig. 3). The degree of connectivity decreases for larger thresholds and the networks become sparser during both seizure and interictal activity (Table I, Fig. 3). Table I reports the number of statistical significant functional network connections (i.e., edges) in the functional network that manifests during epochs of seizure versus during epochs of interictal activity. In parenthesis, we indicate the number of statistical significant edges that are unique during each state (interictal activity vs. seizure). The last column corresponds to the number of statistical significant edges common to both states. Seizure manifests significantly reduced synchronicity compared to interictal state.

As expected the higher the z-score threshold, the lower the number of significant edges in interictal and seizure state (Table I).

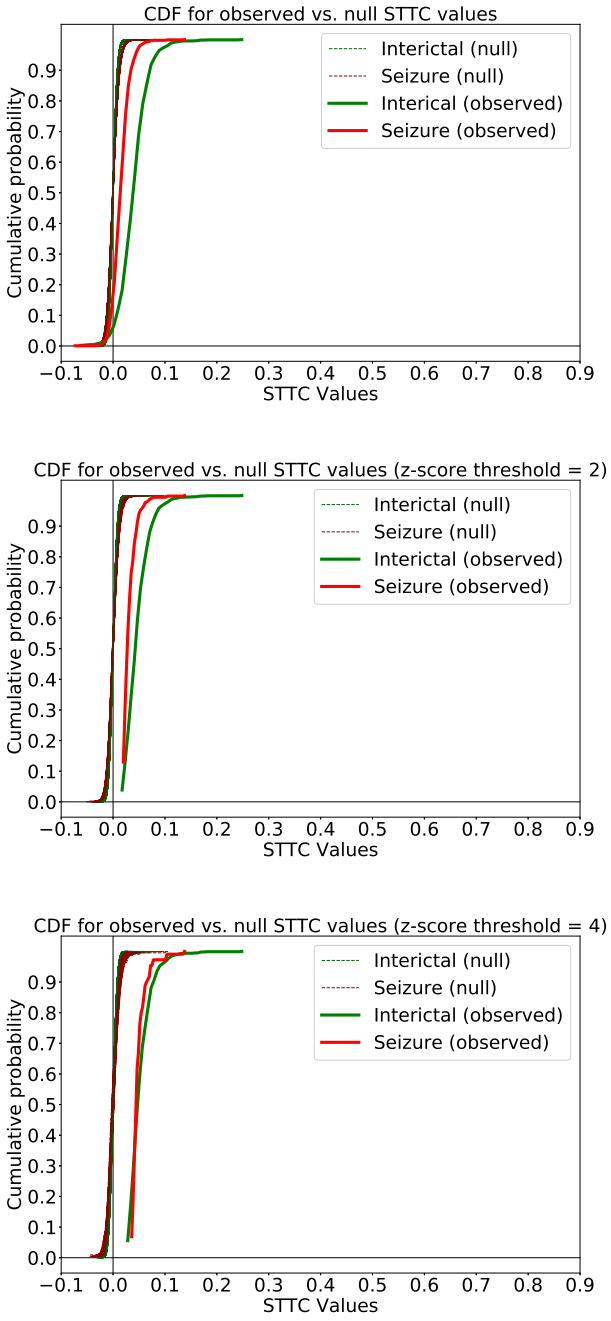

Fig. 1: Distinct pairwise correlation in interictal activity vs. in seizure, for mouse A. The observed STTC values versus null (dotted lines) for the significant edges, in interictal activity and seizure, in green and red color, respectively, at different z-score thresholds. Neuropil patches are not included.

TABLE I: Total number of significant edges for different thresholds, for mouse A. The number of unique edges in each state is reported in parenthesis.Seizure manifests significantly reduced synchronicity compared to interictal epochs. Note that neuropil patches have been excluded.

Threshold	Interictal (Unique)	Seizure (Unique)	Both states
2	2434 (1420)	1063 (49)	1014
4	1976 (1772)	219 (15)	204
6	1405 (1379)	28 (2)	26
8	817 (812)	5 (-)	5
10	441 (439)	2 (-)	2

Functional network size decreases during seizure epochs. This is reflected by the reduced number of statistical significant edges in seizure, compared to interictal activity (Table I) as well as the reduced degree of connectivity (Fig. 6).

Neuropil patches exhibit higher temporal correlation than neurons. Pairs between neuron to neuropil patches exhibit higher STTC values compared to pairs between neurons in epochs of seizure as well as interictal activity (Fig. 8). STTC values between neurons and adjacent neuropil patches (reflecting in some sense the coupling between neuronal activity at the soma and the aggregate activity of inputs/outputs in layer 2/3) are higher compared to values obtained between pairs of neurons. This occurs in both epochs of absence seizures and epochs of normal (interictal) activity. However, the relative strength of STTC correlations during interictal activity versus absence epochs of activity remains the same as described in Fig. 1 (see Fig.8).

Similar trend exists for pairs between neuropil patches and inter-neurons in both seizure and interictal activity (as shown in Fig. 2). Specifically, each point in this scatterplot corresponds to a pair and includes the STTC and mutual information values of this pair. The mutual information (MI) of two random variables is a measure of the mutual dependence between these variables. More specifically, it quantifies the "amount of information" obtained about one random variable through observing the other random variable. Here, the mutual information of a pair of neurons has been estimated using their spike trains at frame level. The interictal activity is in green, while the seizure in red. Pairs between neuropil patches (in blue) tend to have higher STTC values in seizure and in interictal activity compared to pairs between neurons. This trend is prominent for mouse A, where pairs between neuropil patches are located at the tail of the scatterplot with significantly higher STTC values than neuron-neuron pairs. It is clear from Fig. 2 that STTC values are correlated with mutual information.

Functional connectivity abnormalities precede the onset of absence events (first EEG spike of the absence seizure). We identified which STTC "edges" are significant solely during interictal but not in absence epochs, and then followed the aggregate number of co-firing events that occur second by second as a function of time prior to the onset of a seizure in these edges. Fig. 4 shows that the cdf of co-firing events one second prior to the onset of the seizure is identical to the cdf obtained during the seizure. The further away from a seizure onset, the closer to the interictal activity the cdf profile returns (e.g., aggregate number of firing events per window, considering all neurons, for different types of 15-frame windows, namely interictal activity, seizure, and various number of seconds prior to a seizure onset, as shown in Fig. 5). For example, time-windows that start 5-sec prior to a seizure onset display a pattern similar to that of interictal activity (Fig. 5 light green, dotted line), whereas time-windows closer to the seizure onset (See Fig. 5 light green, solid line and Fig. 4 yellow line) display a pattern of activity increasingly similar to seizure.

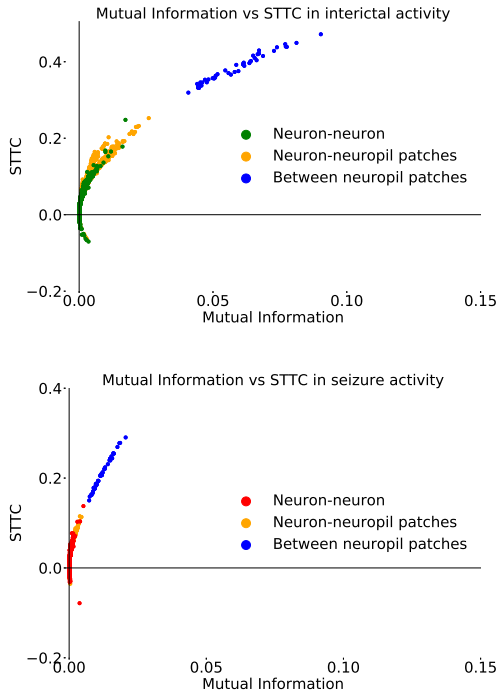

Fig. 2: Scatterplot of mutual informaton versus STTC values for pairs of neurons, as well as for pairs of neuropil patches, for mouse A. Pairs between neuropil patches appear uniformly in blue, whereas pairs between neurons and adjacent neuropil patches appear in orange. STTC values for pairs of neurons are labeled by green and red depending on whether they are obtained for epochs of interictal versus seizure activity, respectively. Pairs between neuropil patches exhibit higher STTC values compared to pairs between neurons in both seizure and interictal activity.

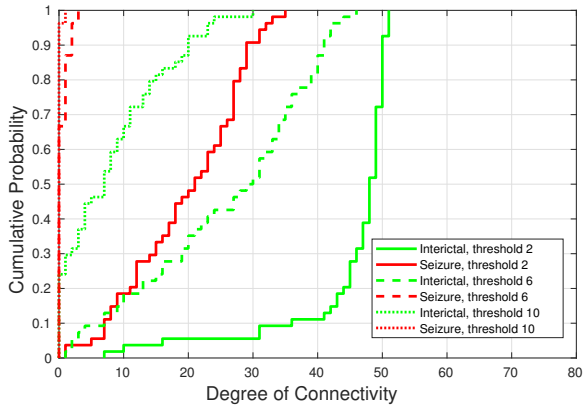

Fig. 3: Degree of connectivity of each neuron for mouse A, considering only the significant neuron-neuron edges, for thresholds equal to 2, 6 and 10 in both interictal and seizure activity. Absence seizures manifest significantly reduced synchronicity compared to interictal activity.

Similar trends are observed when we consider the aggregate activity of neurons who participate in significant STTC pairs only during absence seizure events.

Similar trends are observed in the other mouse. Specifically, Fig. 6 shows the high degree of connectivity of neurons in interictal activity, significantly higher than in seizure, for

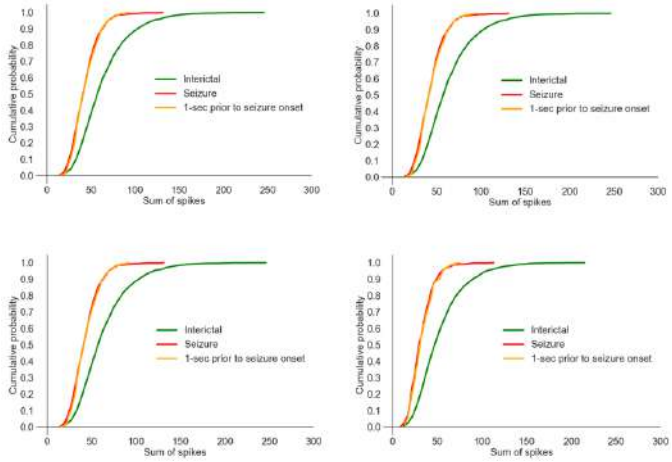

Fig. 4: CDF of the sum of spikes per window for neurons of mouse A that belong in unique neuron-neuron edges of interictal activity, for threshold equal to 2 (left column, first row), 4 (right column, first row), 6 (left column, second row), and 10 (right column, second row).

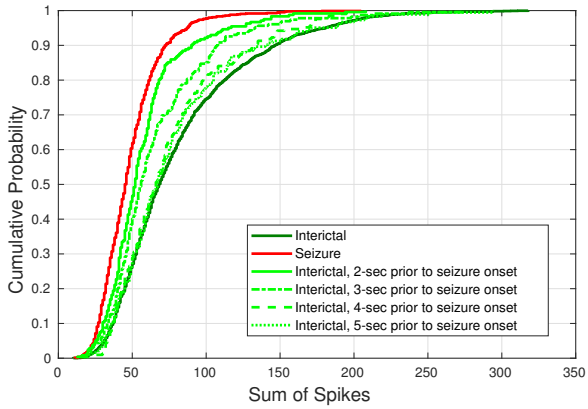

Fig. 5: CDF of the sum of firing events for all neurons of mouse A, for interictal activity (dark green), seizure (red), 2-sec, 3-sec, 4-sec, and 5-sec, prior to seizure onset (solid, dotdashed, dashed and dotted line respectively).

mouse B. For larger thresholds, the functional network in seizure is destroyed. As threshold increases the functional connectivity network obtained during absence seizure epochs gets decimated first, as was seen in mouse A (Fig. 3).

V. Classification of interictal activity vs. seizure

For each neuron, we divide the original time-series in a series of consecutive non-overlapping time windows of 15 frames. Each window is of 1-sec duration. Windows composed of frames of mixed states were excluded from this analysis. There are 2276 and 837 windows, in total, in interictal activity and seizure, respectively, for mouse A. To detect signs of arousal or inactivation of certain neurons, we calculated the average number of spikes in interictal and in seizure activity for each neuron (Fig. 7).

We trained an SVM classifier for identifying the windows of interictal and seizure activity. For each neuron, we considered the number of its spike events per window. To handle the

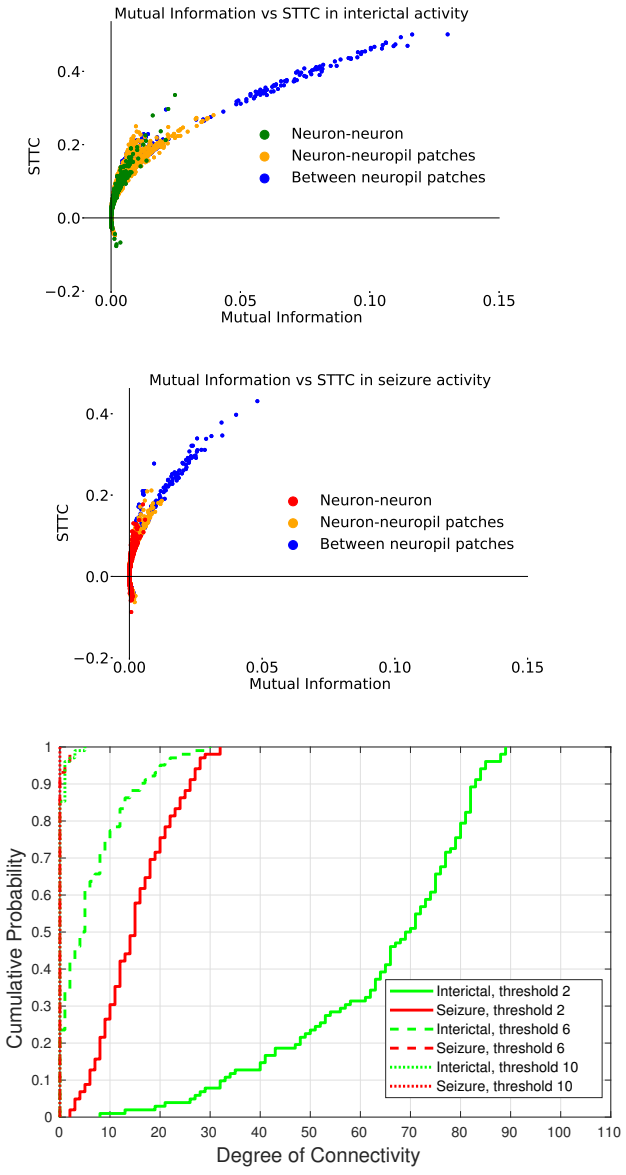

Fig. 6: The first subplot represents the mutual information versus STTC for neuron-to-neuron pairs (green or red), depending on the state, interictal (green; top) vs. seizure activity (red; bottom), as well as for pairs of neuron-to-neuropil patches (orange color) and between neuropil patches (blue color), for mouse B. The second subplot represents the degree of connectivity of each neuron, considering only the significant edges, for thresholds 2,6 and 10 in both interictal and seizure activity, for mouse B.

imbalance between the set of interictal and seizure windows, we applied under-sampling and randomly selected an equal number of samples of interictal windows to use in the training and testing of our model. This process, was repeated for 50 iterations, each time, producing a number of interictal windows equal to the number of seizure windows. At each iteration, a 15-fold cross validation method (14 folds for training, one for testing) was used for evaluating our model. The resulted dataset was used for training and testing. The features of the SVM models were the number of spike events per window of

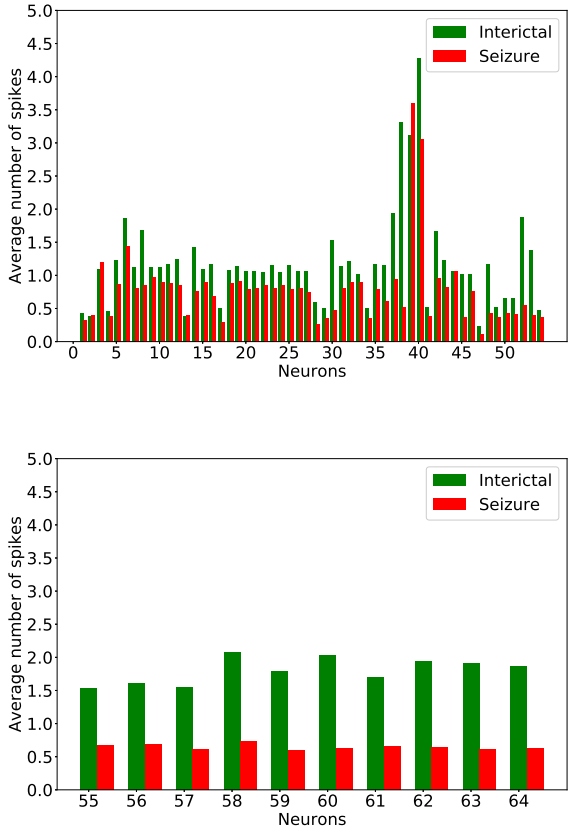

Fig. 7: Average number of spikes per window for interictal activity and seizure, for mouse A. Note that the first subplot includes only neurons and the second only neuropil patches which are the ones with ids in the range of 55-64.

a group of ROIs. The label of a window was its state, namely interictal or seizure. The analysis was performed with a radial kernel (cost 1, gamma 0.005).

An SVM model exhibits the best performance using all 64 ROIs with 67.2% and 88.5% mean accuracy in interictal activity and seizure, respectively (Table II). The sensitivity, which indicates the proportion of the actual ictal windows that are correctly classified as such, is 85.3%. The specificity, which measures the proportion of the interictal periods that are correctly identified as such, is 73%. When we train the SVM model with only the ROI with the largest increase based on the ratio of the difference between mean interictal and ictal firing rate $[(mean_i - mean_s)/mean_s]$, the accuracy in correctly classifying the interictal and seizure windows is 59.7% and 85.6%, respectively (total 72.8%). Sensitivity is 86.6% and specificity is 71.9%. By using only the 30 ROIs with the largest mean activity difference between ictal and interictal states, the mean accuracy in classifying correctly the windows of interictal activity vs. seizure becomes 64.6% and 90%, respectively. The total mean accuracy is 77.3%. This corresponds to the highest accuracy of seizure activity. Adding more neurons in the SVM model does not improve the seizure classification accuracy.

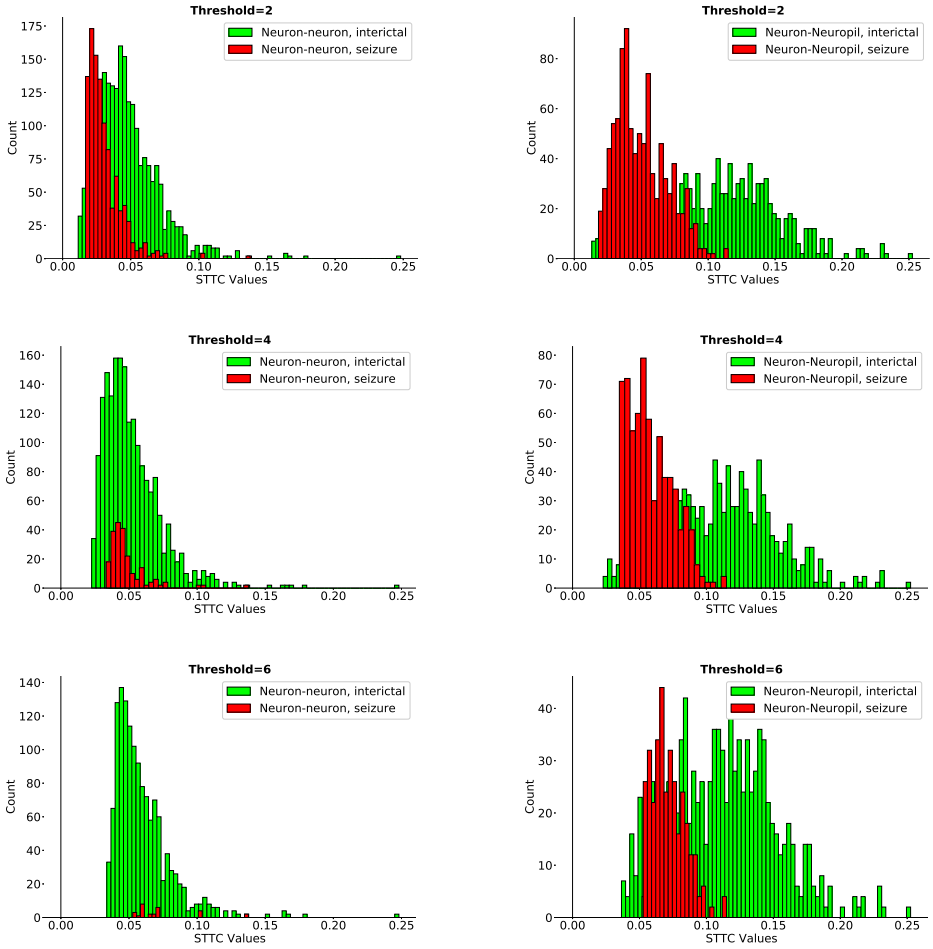

Fig. 8: Statistical significant STTC links between pairs of neurons (neuron-neuron; left column) and between neurons and adjacent neuropil patches (neuron-neuropil; right). Histograms are plotted at different thresholds. Note that the distribution of STTC values is much different in interictal (green) versus absence seizure (red) activity, and this difference is accentuated as threshold increases. The first, second, and third row correspond to thresholds 2, 4, and 6 respectively.

TABLE II: Mean accuracy, sensitivity, and specificity of the 50 training and testing iterations of the SVM model. The nean accuracy is reported in parenthesis for the classification of the interictal and ictal activity, respectively. For each iteration, a number of samples from the set of the interictal windows, equal to number of ictal windows, is selected randomly. The metrics refer to the mean numbers for every testing fold of the 15-fold cross validation.

ROIs	Total Accuracy (Interictal, Ictal)	Sensitivity	Specificity
64	77.9% (67.2%, 88.5%)	85.3%	73%
30	77.3%% (64.6%, 90%)	86.6%	71.9%
1	72.8% (59.7%, 85.6%)	80.5%	68.3%

The "discreet charm" of some neurons. The neurons 53 and 38 have a large discriminating power for classifying the seizure events. For example, with only the neuron 38, the mean accuracy in the classification of seizure and interictal activity windows is 85.6% and 59.7%, respectively.

VI. Conclusions and Future Work

Dense functional networks manifest during interictal activity, while during seizure the functional network connectivity becomes sparse. Specifically, during interictal activity, most of neurons are connected with the others in the field of view, while in absence seizure, the connectivity is reduced substantially, especially for high z-value thresholds. Pairs of neuropil patches exhibit the same seizure versus interictal correlation trends.

An SVM model based on the firing activity of neurons can reasonably accurately classify the interictal activity vs. seizure (e.g., 67.2% for interictal activity, 88.5% for seizure windows). We are in the process of examining further whether the activity of specific groups of neurons, with distinct temporal dynamics, can further improve the classification of seizure events and enable the prediction of seizure events in real-time. Specifically, we examine how STTC analysis can help us define neuronal groups whose activity as a group differs between seizure and interictal state for further improving classification. We observed that the networks change before EEG absence seizure onset, and therefore, there is a time window that makes detection possible. Moreover, the integration of the history of the previous successive windows can further improve the prediction accuracy of seizure events.

Recurrent Quantification-Analysis (RQA) [18], [19] is another technique that can be applied for seizure pattern identi-

fication. The RQA enables the understanding of the behavior of a complex dynamic system (e.g., deterministic, random, chaotic), without making any assumption about the model that governs the system or the data, e.g., linearity, convexity, stationarity. The RQA has several other attractive characteristics: it can handle short time-series, non-stationary data, and is robust to outliers. Here, time-dependent RQA will be performed in small windows moving over the recurrence plot (for different ictal phases) enabling the detection of phase transitions (e.g. determinism-chaos, chaos-chaos). Such efforts aim to form the basis for developing new circuit-based therapeutic strategies targeting specific cell classes.

VII. Acknowledgement

We thank Atul Maheshwari and Jeff Noebels for their help with the EEG interpretation as well as for providing the stargazer mouse line.

References

[1] A. Maheshwari and J. L. Noebels, "Monogenic models of absence epilepsy: windows into the complex balance between inhibition and excitation in thalamocortical microcircuits," *Progress in Brain Research*, vol. 213C, pp. 223–252, 2014.

[2] H. O. Tan, C. A. Reid, P. J. D. F.N Single, C. Chiu, S. Murphy, A. L. Clarke, L. Dibbens, H. Krestel, J. C. Mulley, M. V. Jones, P. H. Seeburg, B. Sakmann, S. Berkovic, R. Sprengel, and S. Petrou, "Reduced cortical inhibition in a mouse model of familial childhood absence epilepsy," *Proceedings of the National Academy of Sciences of the United States of America*, vol. 104, no. 44, pp. 17536–1754, 2007.

[3] S. Feldt, P. Bonifazi, and R. Cossart, "Dissecting functional connectivity of neuronal microcircuits: experimental and theoretical insights," *Trends Neuroscience*, vol. 34, no. 5, pp. 225–236, 2011.

[4] C. S. Cutts and S. J. Eglen, "Detecting pairwise correlations in spike trains: An objective comparison of methods and application to the study of retinal waves," *The Journal of Neuroscience*, vol. 34, no. 43, pp. 14288–14303, 2014.

[5] J. Meyer, A. Maheshwari, J. Noebels, and S. Smirnakis, "Asynchronous suppression of visual cortex during absence seizures in stargazer mice," *Nature Communications*, vol. 9, no. 1, p. 1938, 2018.

[6] J. L. Noebels, X. Qiao, R. T. Bronson, C. Spencer, and M. T. Davisson, "Stargazer: a new neurological mutant on chromosome 15 in the mouse with prolonged cortical seizures," *Epilepsy Research*, vol. 7, no. 2, pp. 129–135, 1990.

[7] A. Maheshwari, W. K. Nahm, and J. L. Noebels, "Paradoxical proepileptic response to nmda receptor blockade linked to cortical interneuron defect in stargazer mice," *Frontiers in Cellular Neuroscience*, vol. 7, p. 156, 2013.

[8] C. J. Lacey, A. Bryant, J. Brill, and J. R. Huguenard, "Enhanced nmda receptor-dependent thalamic excitation and network oscillations in stargazer mice," *Journal of Neuroscience*, vol. 32, no. 32, pp. 11067–11081, 2012.

[9] Z. Barad, O. Shevtsova, G. W. Arbuthnott, and B. Leitch, "Selective loss of ampa receptors at corticothalamic synapses in the epileptic stargazer mouse," *Neuroscience*, vol. 217, pp. 19–31, 2012.

[10] Y. Zhang, M. Mori, D. L. Burgess, and J. L. Noebels, "Mutations in high-voltage-activated calcium channel genes stimulate low-voltage-activated currents in mouse thalamic relay neurons," *Journal of Neuroscience*, vol. 22, no. 15, pp. 6362–6371, 2002.

[11] H. Nersesyan, P. Herman, E. Erdogan, F. Hyder, and H. Blumenfeld, "Relative changes in cerebral blood flow and neuronal activity in local microdomains during generalized seizures," *Journal of Cerebral Blood Flow and Metabolism*, vol. 24, no. 9, pp. 1057–1068, 2004.

[12] P. Polack, I. Guillemain, E. Hu, C. Deransart, A. Depaulis, and S. Charpier, "Deep layer somatosensory cortical neurons initiate spike-and-wave discharges in a genetic model of absence seizures," *Journal of Neuroscience*, vol. 27, no. 24, pp. 6590–6599, 2007.

[13] R. Berman, M. Negishi, M. Vestal, M. Spann, M. H. Chung, X. Bai, M. Purcaro, J. E. Motelow, N. Danielson, L. Dix-Cooper, M. E. E. J. Novotny, R. Constable, and H. Blumenfeld, "Simultaneous eeg, fmri, and behavior in typical childhood absence seizures," *Epilepsia*, vol. 51, no. 10, pp. 2011–2022, 2010.

[14] Y. Aghakhani, A. Bagshaw, C. Bnar, C. Hawco, F. A. F. Dubeau, and J. Gotman, "fmri activation during spike and wave discharges in idiopathic generalized epilepsy," *Brain: A Journal of Neurology*, vol. 127, no. 5, pp. 1127–1144, 2004.

[15] J. N Guo, K. Robert, Y. Chen, M. Negishi, S. Jhun, S. Weiss, J. Hwan Ryu, X. Bai, W. Xiao, E. Feeney, J. Rodriguez-Fernandez, H. Mistry, V. Crunelli, M. Crowley, L. C Mayes, R. Constable, and H. Blumenfeld, "fmri activation during spike and wave discharges in idiopathic generalized epilepsy," *Lancet Neurology*, vol. 15, no. 13, pp. 1336–1345, 2016.

[16] E. Yaksi and R. W. Friedrich, "Reconstruction of firing rate changes across neuronal populations by temporally deconvolved ca2+imaging," *Nature Methods*, vol. 3, no. 5, pp. 377–383, 2006.

[17] J. T. Vogelstein, A. M. Packer, T. A. Machado, T. Sippy, B. Babadi, R. Yuste, and L. Paninski, "Fast nonnegative deconvolution for spike train inference from population calcium imaging," *Journal of Neurophysiology*, vol. 104, no. 6, pp. 3691–3704, 2010.

[18] N. Marwan, M. C. Romano, M. Thiel, and J. Kurths, "Recurrence plots for the analysis of complex systems," *Physics Reports*, vol. 438, pp. 237–329, 2007.

[19] N. Marwan, M. Thiel, and N. R. Nowaczyk, "Cross recurrence plot based synchronization of time series," *Nonlinear Processes in Geophysics*, vol. 9, no. 3, pp. 325–331, 2002.